Draft version January 13, 2021
Typeset using LaTeX **manuscript** style in AASTeX63

arXiv:2101.03732v2 [astro-ph.GA] 12 Jan 2021

Role of Polycyclic Aromatic Hydrocarbons on the Cosmic-Ray ionization rate in the Galaxy

Gargi Shaw[1] and G. J. Ferland[2]

[1]*Department of Astronomy and Astrophysics, Tata Institute of Fundamental Research*

Homi Bhabha Road, Navy Nagar, Colaba, Mumbai 400005, India

[2]*Department of Physics and Astronomy, University of Kentucky*

Lexington, KY 40506, USA

Submitted to ApJ

ABSTRACT

The cosmic-ray ionization rate (ζ, s^{-1}) plays an important role in the interstellar medium. It controls ion-molecular chemistry and provides a source of heating. Here we perform a grid of calculations using the spectral synthesis code CLOUDY along nine sightlines towards, HD 169454, HD 110432, HD 204827, λ Cep, X Per, HD 73882, HD 154368, Cyg OB2 5, Cyg OB2 12. The value of ζ is determined by matching the observed column densities of H_3^+ and H_2. The presence of polycyclic aromatic hydrocarbons (PAHs) affects the free electron density, which changes the H_3^+ density and the derived ionization rate. PAHs are ubiquitous in the Galaxy, but there are also regions where PAHs do not exist. Hence, we consider clouds with a range of PAH abundances and show their effects on the H_3^+ abundance. We predict an average cosmic-ray ionization rate for H_2 ($\zeta(H_2)$)= $(7.88 \pm 2.89) \times 10^{-16}$ s^{-1} for models with average

Corresponding author: Gargi Shaw
gargishaw@gmail.com, gary@g.uky.edu

Galactic PAHs abundances, (PAH/H $=10^{-6.52}$), except Cyg OB2 5 and Cyg OB2 12. The value of ζ is nearly 1 dex smaller for sightlines toward Cyg OB2 12. We estimate the average value of $\zeta(H_2)= (95.69 \pm 46.56) \times 10^{-16}$ s^{-1} for models without PAHs.

Keywords: ISM: molecules, ISM: abundances, ISM: cosmic rays, ISM: PDR

1. INTRODUCTION

Cosmic rays (CR) are high-energy particles mostly made of protons whose energy ranges from few MeV to few GeV. They penetrate deep into interstellar clouds and produce a primary ionization and a cascade of secondary ionizations (Spitzer & Tomasko 1968). The free electrons they produce heat the gas, and deep in the cloud they control the ion-molecular chemistry network in the absence of other ionizing sources. Hence it is very important to determine the cosmic-ray ionization rate (ζ) for such environments. Several groups estimated the value of ζ based on the abundances of various molecules such as HD (O'Donnell & Watson 1974), H_3^+ (Indriolo & McCall 2012; Neufeld & Wolfire 2017). Interestingly, the value differs depending on the molecule involved. In the diffuse clouds, ζ is determined from the observed column densities of H_3^+ since it undergoes simple chemical reactions (McCall et al. 2003). However, H_3^+ undergoes a complex chain of chemical reactions in dense clouds (Dalgarno 2006) and the value of ζ is lower than that of diffuse clouds.

The current estimate of the average value of ζ ($3.5^{+5.3}_{-3.0} \times 10^{-16}$ s^{-1}) in the galaxy is provided by McCall et al. (2003), Indriolo et al. (2007), Indriolo & McCall (2012) based on H_3^+ observations. Similar value of (5.3±1.1) $\times 10^{-16}$ s^{-1} has been reported by Neufeld & Wolfire (2017). Earlier to the H_3^+ revolution, the value of ζ had been derived using other molecules, such as HD and OH (O'Donnell & Watson 1974; Black & Dalgarno 1977; Hartquist et al. 1978; Federman et al. 1996). However, H_3^+ gives a higher value than other methods, and the value of ζ varies by nearly an order of magnitude across the Galaxy Indriolo & McCall (2012). Le Petit et al. (2016) and Oka et al. (2019) have reported even higher values in the central molecular zone of the Galaxy. In addition, Shaw et al. (2016) and Rawlins et al. (2018) have reported higher value of ζ in high-redshift H_2 bearing Damped Lyman alpha absorbers.

The H_3^+ method relies on measurements of the column density of that molecular ion and needs the electron density in the H_3^+ region to derive ζ. It is not possible to measure the electron density directly, so indirect assumptions, described in the next section, have been made. Dalgarno (2006) and Neufeld & Wolfire (2017) have examined the chemical reactions which affect the H_3^+. Here we examine the effects of polycyclic aromatic hydrocarbons (PAHs) on the electron density and determine its impact on determining the value of ζ.

This paper is organized in the following manner: in Section 2, we describe the H_3^+ chemistry and the role of electron density. Our grid of numerical simulations of nine sightlines and the results are presented in Sections 3 and 4, respectively. Discussions and Summary are given in section 5 and 6, respectively.

2. H_3^+ CHEMISTRY AND ELECTRON DENSITY

2.1. *Observations and analytical analysis*

The molecular ion H_3^+ is a very important species which can be used to estimate the cosmic-ray ionization rate (McCall et al. 1998, 2003). In the diffuse interstellar clouds, H_3^+ is mainly formed by the cosmic ray ionization of H_2,

$$H_2 + CR = H_2^+ + e^- \tag{1}$$

followed by proton abstraction reaction producing

$$H_2^+ + H_2 = H_3^+ + H. \tag{2}$$

Whereas, H_3^+ is destroyed mainly by dissociative recombination processes,

$$H_3^+ + e^- = H + H + H \text{ or } H_2 + H \ . \tag{3}$$

Process 2 is very slow, so in steady state we can write,

$$\zeta(H_2)n(H_2) = k_e n(e^-)n(H_3^+). \tag{4}$$

Here, $\zeta(H_2)$ and k_e represent the cosmic-ray ionization rate of H_2 and the electron-recombination co-efficient of H_3^+, respectively. The terms $n(X)$ represent the number density (cm^{-3}) of species X.

For a uniform cloud with length L (cm), the densities can be converted into column densities N (cm^{-2}) and equation 4 takes the form

$$\zeta(H_2) = k_e n(e^-) N(H_3^+)/N(H_2)\ [s^{-1}]. \tag{5}$$

Defining the molecular fraction as

$$f = 2N(H_2)/N(H), \tag{6}$$

one gets

$$\zeta(H_2) = 2k_e n(_e) N(H_3^+)/fN(H)[s^{-1}]. \tag{7}$$

Indriolo & McCall (2012) have observed H_3^+ in absorption along 50 diffuse sightlines and derived the column densities needed to evaluate equation 7. The observed column densities of H_3^+ are distributed over a range $5{\times}10^{13}$ to $3.7{\times}10^{14}$ cm^{-2}. An electron density is required to derive the cosmic-ray ionization rate.

Indriolo et al. (2007) and Indriolo & McCall (2012) derived $\zeta(H_2)$ by assuming $f = 0.67$. In reality, a large range in f is possible so there is significant uncertainty in estimating the values of f and n(H). van Dishoeck & Black (1986) showed that in diffuse clouds, nearly all carbon is singly ionized. Indriolo et al. (2007) further assumed that in diffuse clouds, nearly all electrons are produced via the ionization of C to C^+ and C/H should approximate the electron fraction, e^-/H, that is, $n_e = n(C^+)$. They assumed a single average value, $n_e/n(H) = 1.4 \times 10^{-4}$, for all of their calculations and derived a high value for $\zeta(H_2)$ compared to earlier estimates.

2.2. *Numerical methods*

Diffuse clouds show structures like photodissociation regions (PDR) (Tielens & Hollenbach 1985). Hence, we first investigate the above-mentioned assumptions regarding electron density for a standard PDR model. Then we perform detailed numerical simulations of nine sightlines, which are discussed later, to estimate an average cosmic-ray ionization rate.

All the models presented here are calculated using spectroscopic simulation code, CLOUDY (Ferland et al. 2013, 2017; Shaw et al. 2005, 2020). For this work, we have updated the following rate

coefficients for the reactions involving H_3^+,

$$H_3^+ + CO = H_2 + HCO^+ \tag{8}$$

$$H_3^+ + CO = H_2 + HOC^+ \tag{9}$$

$$H_3^+ + O = H_2 + OH^+ \tag{10}$$

$$H_3^+ + N_2 = H_2 + HN_2^+. \tag{11}$$

These rates are from Klippenstein et al. (2010), and Rakshit (1982), respectively. The reaction rates for equation 2 and 3 are taken from Theard & Huntress (1974) and McCall et al. (2004), respectively. McCall et al. (2004) provides the total dissociative recombination rate for the products (eqn.3). UMIST RATE12 (http://udfa.ajmarkwick.net) provides a branching ratio of 0.53 : 1. The branching ratios of any product reaction rate is important. Though a branching ratio 0.53 : 1 works for the models discussed here, it introduces instability in chemical networks for primordial IGM models. In CLOUDY, we use a branching ratio 0.25 : 1 . For other atomic, ionic, and molecular processes, CLOUDY utilises five distinct databases (Porter et al. 2012; Lykins et al. 2015; Shaw et al. 2005).

We use the size-resolved PAHs, distributed in 10 size bins, and the size distribution of the PAHs is taken from Abel et al. (2008) with minimum and maximum radii of 0.00043 μm (30 C atoms) and 0.0011 μm (500 C atoms), respectively. Non-equilibrium heating is important for these small grains, and we include this effect in our calculations. Besides this, we also consider the photoelectric effect as well as charge exchange of PAHs with atoms/ions and electrons to determine the charge of the PAHs. Inner-shell photoionization and the Auger effect of grains and PAHs are also treated following Weingartner et al. (2006). We include the opacity of both neutral and charged PAHs in our calculation with opacities according to Li & Draine (2001), who adopted a thermal approximation. Grains have a net charge, and so affect the density of free electrons. Our treatment of this physics is described in Abel et al. (2008). In all the models discussed here (if not specified), the temperature is determined from heating and cooling balance involving various terms (Ferland et al. 2017).

2.3. *Ionization structure, electron density and Carbon to Hydrogen ratio*

We test the assumptions about the electron density by running the standard Leiden PDR models (F1, F2, F3, F4) (Röllig et al. 2007) and finding the predicted H_3^+. We find column densities for the F1, F2, F3, and F4 models to be 9.8×10^{14}, 3.29×10^{14}, 1.4×10^{13}, 1.09×10^{13} cm^{-2} respectively. All these models extend up to Av=10. However, the samples of diffuse cloud considered by Indriolo & McCall (2012) extend less than Av=10. Hence as a next step, we run the F1 and F2 models stopping at $N(H_3^+) = 10^{13.8}$ cm^{-2} and check the corresponding Av. We find Av= 3.16 and 6.9 for F1 and F2 models, respectively. Hence we consider F1 as a standard model for further investigation as many of the clouds of the Indriolo & McCall (2012) sample have Av in these ranges, and examine the basis for estimates of the electron fraction to be equal to C/H.

The model F1 is a constant temperature PDR model at 50 K with hydrogen density 10^3 cm^{-3} and impinging radiation field with a strength of 17.0 G0, where G0 is the widely used standard FUV radiation field measured in units of $1.6\times10^{\ 3}$ ergs cm $^{-2}$s^{-1} (Tielens & Hollenbach 1985). Details of this model is discussed in Röllig et al. (2007). The only difference between Röllig et al. (2007) and this work is that here we consider ISM gas phase abundances (Cowie & Songaila 1986; Savage & Sembach 1996; Meyer et al. 1998; Snow et al. 2007), ζ(H)= $2\times\ 10^{-16}$ s^{-1}, and extend the model till $N(H_3^+) = 10^{13.8}$ cm^{-2}. Our work does not use the simplified expression for electron density as suggested by Indriolo & McCall (2012). Instead, we use a detailed chemical network with appropriate microphysics (Abel et al. 2008; Ferland et al. 2013; Shaw & Ferland 2020).

Fig. 1 shows the density of C^0, C^+, H^+, S^+, H_3^+, and e^- as a function of Av. It is clear from the plot that *a*) all the carbon is not in C^+ throughout the entire cloud. Carbon is mostly in the form of C^+ at shallower Av and decreases as Av increases. *b*) all the electrons are not contributed by C^+. Ionization of H^+, S^+, and other metals also contribute to the total electron density. Hence, e^-/H is not equal to C/H. For this model e^-/H > C/H.

Fig. 2 shows the electron fraction as a function of $n(H_3^+)$ for this model. Initially $n(e^-)/n(H)$ is higher than the assumed C/H abundance ratio of $2.5\times\ 10^{-4}$. This is because ions of H, S, Mg provide

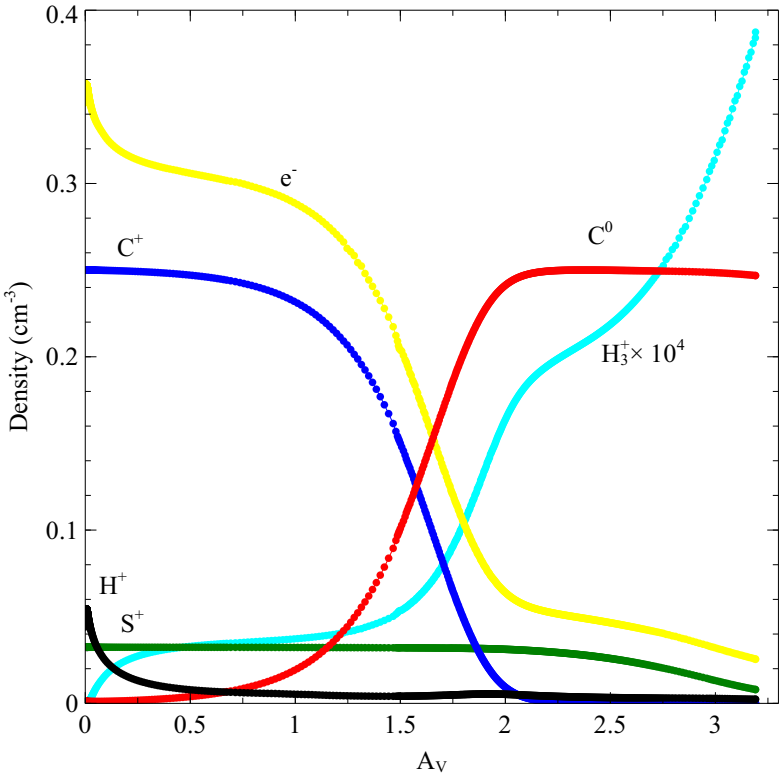

Figure 1. Ionization structure for model F1. Density of C^0, C^+, H^+, S^+, H_3^+, and e^- are plotted as a function of Av.

electrons besides C. On top of this, the electron fraction decreases nearly by a factor 10 at higher Av where H_3^+ forms. This would have a significant impact on the estimate of ζ (see equation 7).

2.4. *Effect of physical conditions on electron density*

From PDR models it is known that other elements besides C also contribute to the total electron density depending on the density, impinging radiation fields and metallicity. Additionally, grains can add or remove electrons from the gas. PAHs also change the electron density due to its high electron affinity (Carelli et al. 2013). Jenkins (2009) has also shown that metals are depleted in different amounts across the Galaxy. On top of this, there is an additional positive feedback contribution of electrons from the cosmic-ray ionization of H, ζ (H), since the number of secondary electrons that are produced by a primary ionization depends on the electron fraction. It is to be noted here that generally $\zeta(\mathrm{H}) = 0.5 \times \zeta(\mathrm{H_2})$. In light of these facts, here we show the effects of various physical conditions on electron density.

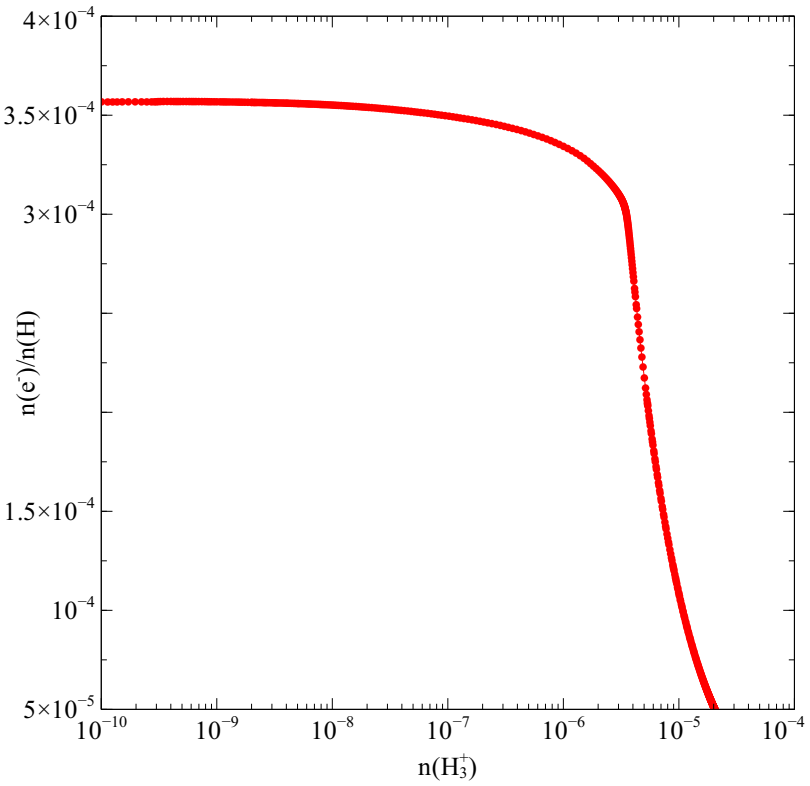

Figure 2. $n(\mathrm{e}^-)/n(\mathrm{H})$ is plotted as a function of $n(\mathrm{H}_3^+)$ for model F1.

As a simple test, we ran the Leiden F1 model varying single parameters while keeping all the other parameters the same. Unlike the canonical Leiden PDR model, we include PAHs. We varied the radiation field and the cosmic-ray ionization rate ζ. Fig. 3 shows the electron densities as a function of Av with a radiation field with strength 85 G0 (cyan), ζ(H)= 2$\times$ 10^{-15} s^{-1} (green), and PAHs (blue). The default case is shown with the red solid line. For these cases, the shape of the $n(\mathrm{e}^-)/n(\mathrm{H})$ vs. $n(\mathrm{H}_3^+)$ plot looks similar but the value of $n(\mathrm{e}^-)/n(\mathrm{H})$ is higher. Earlier Shaw et al. (2008) showed that the grain physics plays an important role in determining the value of ζ. Small grains neutralize ions and remove free electrons. They also extinguish the FUV radiation field, and hence influence the deduced value of ζ. Indriolo & McCall (2012) assumed a single average value (1.4 $\times 10^{-4}$) for e^-/H. For model F1 the value of total hydrogen density is 10^3 cm^{-3}. Hence, their derived electron density would be 0.14 cm^{-3} throughout the entire cloud. Considering all these facts,

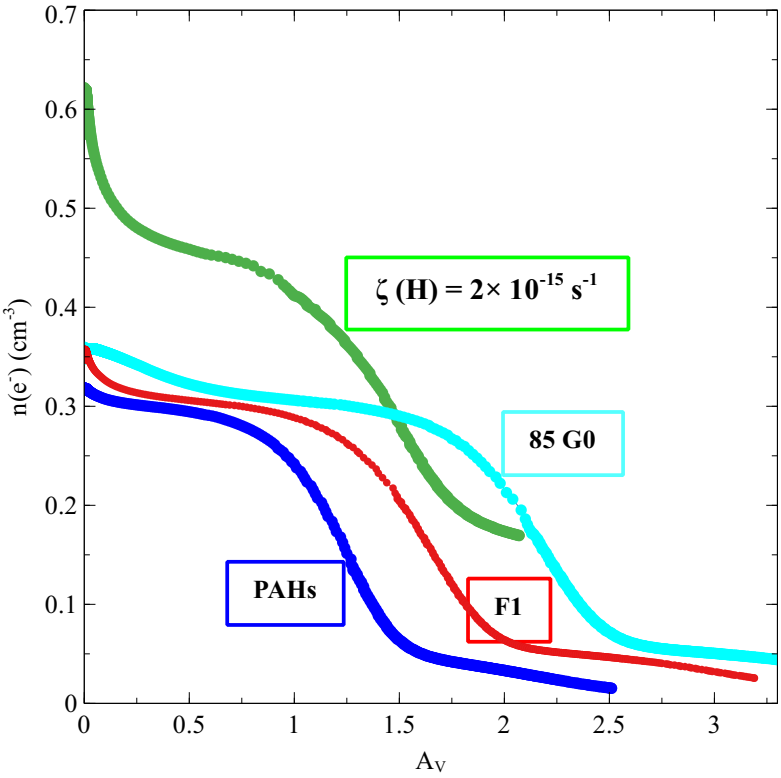

Figure 3. The red, cyan, green, blue solid lines show $n(e^-)$ as a function of Av for default F1, and with increased radiation field, increased ζ(H), and with PAHs, respectively. All clouds have a thickness that reproduces the same column density in H_3^+ ($10^{13.8}$ cm^{-2}).

we revisit the value of ζ by modelling various sight-lines with observed column densities of H_3^+ and H_2, using detailed numerical simulation.

3. GRIDS OF MODELS

Here we present numerical simulations of nine sightlines from Indriolo & McCall (2012), namely, HD 169454, HD 110432, HD 204827, λ Cep, X Per, HD 7388, HD 154368, Cyg OB2 5, and Cyg OB2 12. To minimize uncertainties in modelling, we choose only those sightlines for which the density is derived from observed C_2 levels (Sonnentrucker et al. 2007; Rachford et al. 2002). All these sightlines have reported H_2 observations and E(B-V). We assume that the classical grains have a Mathis et al. (1977) size distribution. Hence, we consider R=3.2 and calculate Av as 3.2× E(B-V). Very little is known about the presence or absence of PAHs along these sightlines.

Table 1 lists all the observed information for the nine sightlines modelled here. For each sightline, we run a grid of models with varying radiation field and ζ(H) in a step of 0.5 dex. We specify the radiation field in terms of the standard Galactic Habing radiation field (G0). The shape of the SED is that given by Black (1987) but assuming an extinction of 1 to 4 Ryd radiation as this is highly absorbed in ISM. Based on the observed H_3^+ and H_2 column density ($\pm$ 1σ) contours we estimate $\zeta(H_2)$.

In Section 2.4 we mention that the electron density depends on the presence of PAHs. PAHs have been detected in various places of our Galaxy with large abundances. However, there are some regions, like the ionized part of the Orion Bar (Sellgren et al. 1990) where PAHs do not exist. In NGC 7023 NW (Montillaud et al. 2013), PAHs with less than 50 Carbon atoms are not present. Hence, we perform two sets of calculations for these sightlines. In one set we do not include PAHs while in the other set we include PAHs. Tielens (2008) has determined the abundances of C locked up in PAHs containing 20–100 C atoms as 14 parts per million H atom. As the amount of PAHs is not exactly determined, we consider three different amount of PAHs depending on Tielens (2008), PAH_{lo}, PAH_{avg}, and PAH_{hi}. The number of PAHs per hydrogen for PAH_{lo}, PAH_{avg}, and PAH_{hi} are $10^{-6.85}$, $10^{-6.52}$, and $10^{-6.15}$, respectively.

4. RESULTS

In this section, we present our results for nine sightlines using detailed numerical simulations. We create contour plots showing column densities of H_3^+ and H_2 as functions of X_{CR} and radiation field intensity (in terms of G0). Here, $\zeta(H) = 2{\times}X_{CR} \times 10^{-16}$ s^{-1}.

Fig. 4, Fig. 6, Fig. 8, Fig. 10, Fig. 12, Fig. 14, Fig. 16, Fig. 18, and Fig. 20 show contour plots of H_3^+ and H_2 column densities as a function of X_{CR} and radiation field (in terms of G0) for HD 169454, HD 110432, HD 204827, λ Cep, X Per, HD 73882, HD 154368, Cyg OB2 5, Cyg OB2 12 without any PAHs, respectively. The black and blue solid lines represent contour plots of column densities for H_3^+ and H_2, respectively. Whereas, the filled areas with gray and cyan represent observed column density values, for H_3^+ and H_2, $\pm$ 1 σ.

Table 1. list of all the observed information for the nine sightlines modelled

Objects	E(B-V)	E(B-V)	Density	Density	$N(H_3^+) \pm 1\sigma$	$N(H_2) \pm 1\sigma$
	mag	Ref.	cm^{-3}	Ref.	10^{13} cm^{-2}	10^{20} cm^{-2}
HD 169454	1.12	1	300	2	5.93 ± 0.34	16.60 ± 8.37
HD 110432	0.51	3	140	2	5.22 ± 0.17	4.37 ± 0.29
HD 204827	1.11	1	450	2	19.00 ± 2.54	20.90 ± 10.20
λ Cep	0.57	2	115	2	7.58 ± 1.17	6.88 ± 0.48
X Per	0.59	2	325	2	7.34 ± 0.92	8.38 ± 0.89
HD 73882	0.70	4	520	2	9.02 ± 0.50	12.90 ± 2.39
HD 154368	0.78	4	240	2	9.37 ± 1.32	14.40 ± 3.99
Cyg OB2 5	1.99	5	225	2	24.00 ± 3.29	15.20 ± 7.39
Cyg OB2 12	3.35	5	300	2	34.30 ± 5.89	80.00 ± 69.10

NOTE—Ref. (1) Thorburn et al. (2003), (2) Sonnentrucker et al. (2007), (3) Rachford et al. (2002), (4) Rachford et al. (2009), (5) McCall et al. (2002)

In the same manner, Fig. 5, Fig. 7, Fig. 9, Fig. 11, Fig. 13, Fig. 15, Fig. 17, Fig. 19, and Fig. 21 show Contour plot of column densities for H_3^+ and H_2 as a function of X_{CR} and radiation field (in terms of G0) with PAH_{avg} for HD 169454, HD 110432, HD 204827, λ Cep, X Per, HD 73882, HD 154368, Cyg OB2 5, Cyg OB2 12, respectively . Here also the black and blue solid lines represent contour plots of column densities for H_3^+ and H_2, respectively. Whereas, the filled areas with gray and cyan represent observed column density values, for H_3^+ and H_2, $\pm$ 1 σ.

Table 2 lists our findings. The second column of Table 2 shows the predicted value of $\zeta(H_2)$ without considering PAHs in the chemical network. It is clear that without PAHs, except for Cyg OB2 12, most of the sources have $\zeta(H_2) > 10^{-16}$ s^{-1}. We estimate an average value of $\zeta(H_2)$= (95.69 ± 46.56) $\times$ 10^{-16} s^{-1} for models without PAHs.

The third column shows the predicted value of $\zeta(H_2)$ with the lower PAH abundance, PAH_{lo} in the chemical network. The presence of PAHs causes the electron density to decrease and the derived value of $\zeta(H_2)$ to decrease. Adding PAHs causes the derived strength of the radiation field to increase. We

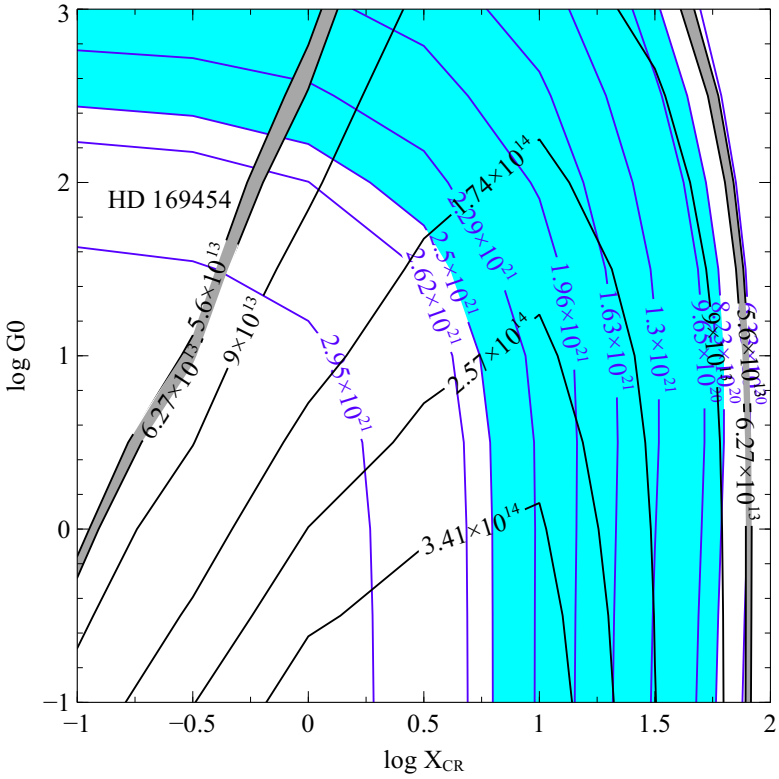

Figure 4. Contour plot of H_3^+ and H_2 as a function of X_{CR} and radiation field (in terms of G0) for HD 169454. The black and blue solid lines represent contour plots of column densities for H_3^+ and H_2, respectively. The filled areas represent observed column density values $\pm$ 1 σ.

estimate an average value of $\zeta(H_2)$= (75.08 $\pm$ 39.90) $\times$ 10^{-16} s^{-1} for models with PAHs abundance, PAH_{lo}, except Cyg OB2 5 and Cyg OB2 12.

The fourth and fifth columns show the predicted value of $\zeta(H_2)$ with the PAHs abundances PAH_{avg} and PAH_{hi}, respectively. As expected, the value of $\zeta(H_2)$ decreases further and the derived radiation field also increases. Our contour plots not only provide an estimate of $\zeta(H_2)$ but also an estimate of the prevailing radiation field in terms of G0. The estimated average values of $\zeta(H_2)$ for these two cases are (7.88 $\pm$ 2.89) $\times$ 10^{-16} s^{-1} and (6.50 $\pm$ 3.06) $\times$ 10^{-16} s^{-1}, except Cyg OB2 5 and Cyg OB2 12. Column six lists the predicted values of $\zeta(H_2)$ by Indriolo & McCall (2012) for comparison. Except for the two Cyg OB2 associations, the values of $\zeta(H_2)$ matches with that predicted by Indriolo & McCall (2012) within the error bars when PAH_{avg} are considered. We predict $\approx$ 1 dex smaller $\zeta(H_2)$ for the Cyg OB2 12 association than predicted by Indriolo & McCall (2012).

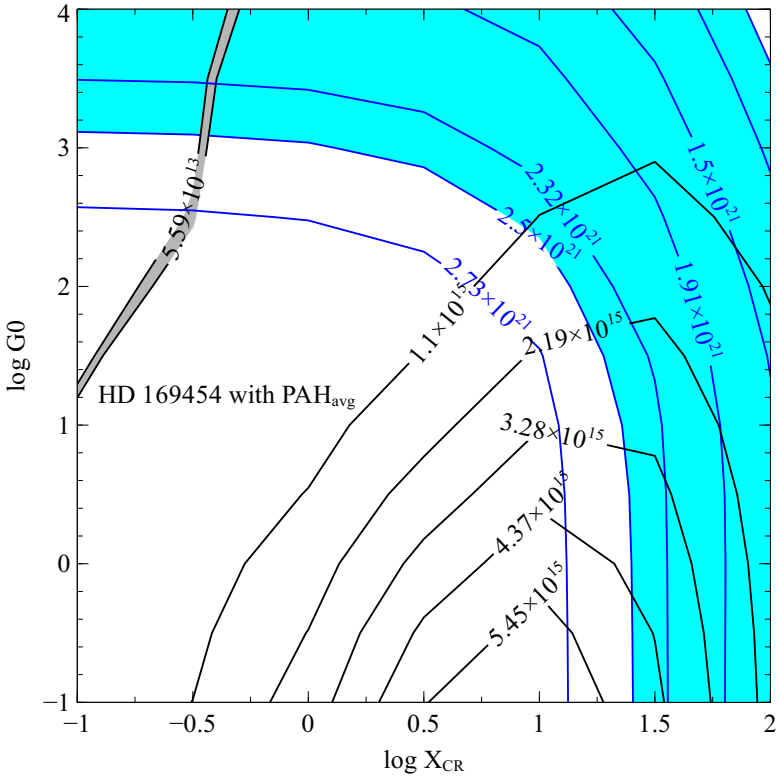

Figure 5. Contour plot of H_3^+ and H_2 as a function of X_{CR} and radiation field (in terms of G0) for HD 169454 with PAHs$_{avg}$. The black and blue solid lines represent contour plots of column densities for H_3^+ and H_2, respectively. The filled areas represent observed column density values $\pm$ 1 σ.

5. DISCUSSIONS

Neufeld & Wolfire (2017) have also performed detail numerical simulations of 7 sightlines based on observed column densities of H_3^+ and H_2 and reported an average value of (5.3$\pm$1.1) $\times$ 10^{-16} s^{-1}. They have included PAHs in their calculations but didn't vary their abundance. It is very important to estimate the amount of PAHs since the value of the observed column densities of H_3^+ and H_2 and ζ depends on it significantly. To illustrate this, we examine the effects of a range of PAH abundances on the molecular abundances in the cloud along the sightline to λ Cep. As a baseline model we choose the radiation field ($10^{3.3}$ G0) and $\zeta(H_2)$ (6.0×10^{-16} s^{-1}), one of the possible solutions for the PAH$_{avg}$ case described above. Fig.22 shows the results of varying the PAH abundance. The red and blue solid lines represent the predicted column densities for H_3^+ and H_2, respectively. The red and

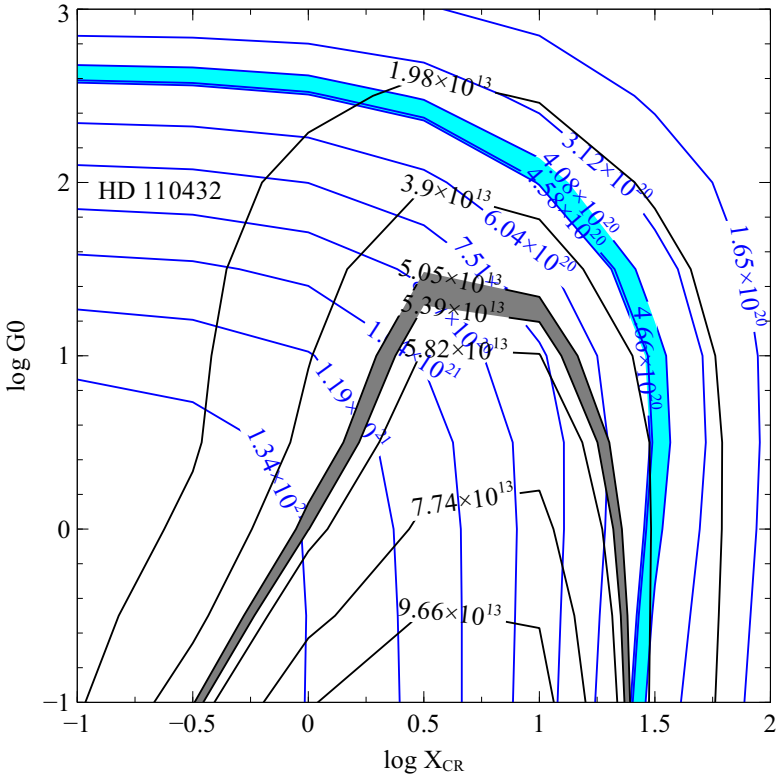

Figure 6. Contour plot of H_3^+ and H_2 as a function of X_{CR} and radiation field (in terms of G0) for HD 110432. The black and blue solid lines represent contour plots of column densities for H_3^+ and H_2, respectively. The filled areas represent observed column density values $\pm$ 1 σ.

blue solid dashed-lines represent respective observed column density values $\pm$ 1 σ. It is clear that a factor of 2 change in the PAHs abundances will predict column densities beyond observed range.

We notice that HD 169454, HD 204827, and the Cyg OB2 12 associations which have higher E(B-V) than the rest of the sample, predicts smaller value of $\zeta(H_2)$ than the rest with high PAHs abundances, PAH_{hi}. A similar dependence on A_V was also reported by Neufeld & Wolfire (2017). Though we can compare the predicted values of $\zeta(H_2)$, observed values of the corresponding radiation field are not available. Our typical derived values of G0 significantly higher than the ISM background, typically G0 10 to 500, consistent with the clouds being near bright stars.

6. SUMMARY

We have used the spectral synthesis code CLOUDY (Ferland et al. 2017) to create detailed simulations of the nine sightlines towards HD 169454, HD 110432, HD 204827, λ Cep, X Per, HD 73882,

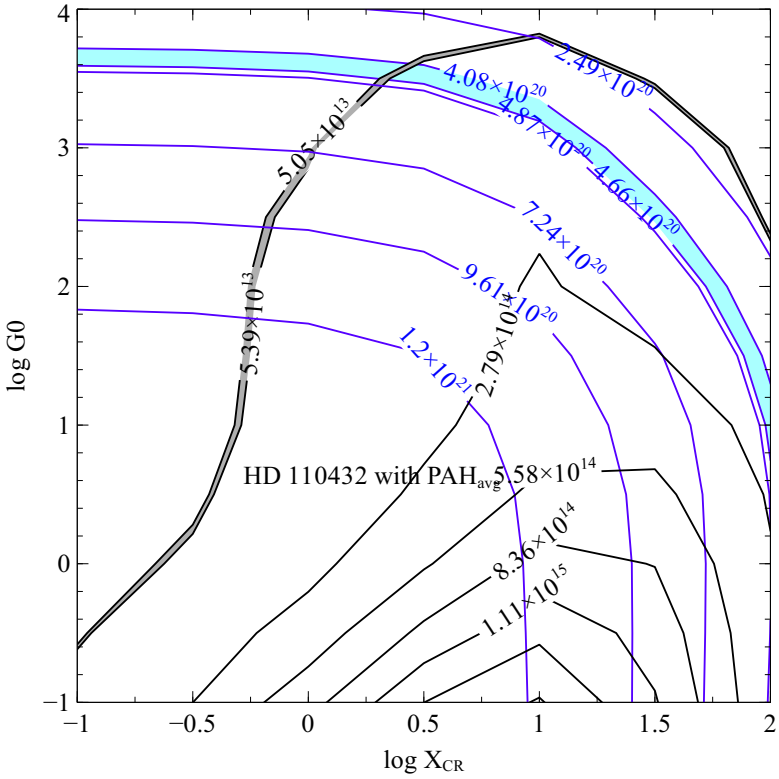

Figure 7. Contour plot of H_3^+ and H_2 as a function of X_{CR} and radiation field (in terms of G0) for HD 110432 with PAH_{avg}. The black and blue solid lines represent contour plots of column densities for H_3^+ and H_2, respectively. The filled areas represent observed column density values $\pm$ 1 σ.

HD 154368, Cyg OB2 5, Cyg OB2 12 and determine the value of $\zeta(H_2)$ based on the observed H_3^+ and H_2 column densities $\pm$ 1 σ. Our goal is to determine the cosmic-ray ionization rate. We also check how sensitive the derived value is to physical assumptions since, as pointed out by Dalgarno (2006), there are many details in the chemistry that affect the derived quantities.

The electron density plays a pivotal role in determining $\zeta(H_2)$. The physical structure of the clouds along these sightlines is similar to a PDR. Hence we first study the electron density and its dependence on various parameters for a standard PDR model, model F1 of the 2006 Leiden PDR workshop Röllig et al. (2007). Then we perform detailed grid calculations for these nine sightlines. The cloud densities are derived from observed C_2 levels (Sonnentrucker et al. 2007; Rachford et al. 2002) and the cloud thicknesses are set from the observed E(B-V).

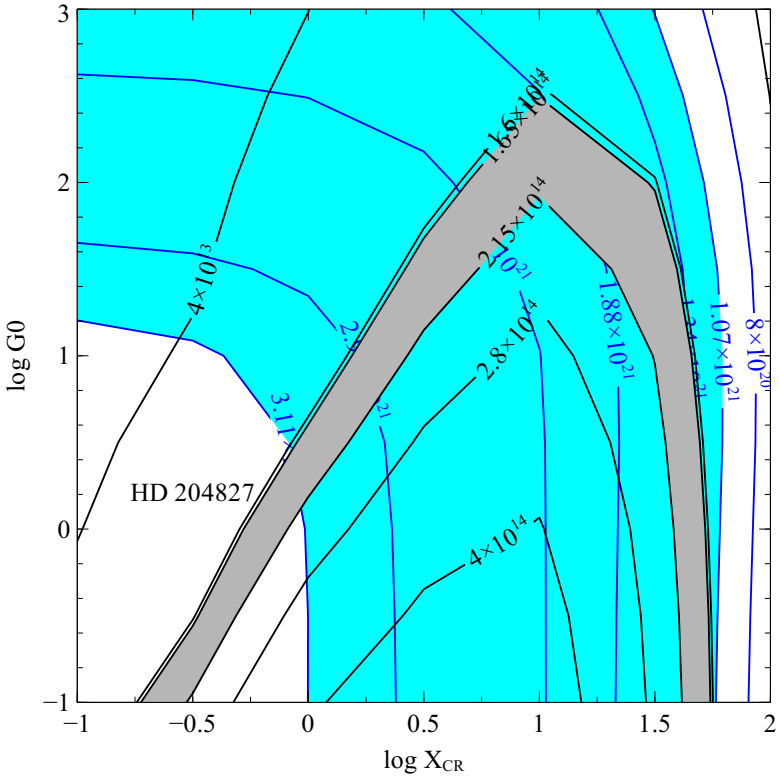

Figure 8. Contour plot of H_3^+ and H_2 as a function of X_{CR} and radiation field (in terms of G0) for HD 204827. The black and blue solid lines represent contour plots of column densities for H_3^+ and H_2, respectively. The filled areas represent observed column density values $\pm$ 1 σ.

Very small grains or large molecules can become charged and affect the free electron density and derived cosmic-ray ionization rate. Although PAHs are very important, their presences or absence is difficult to determine from absorption-line data and we know that there are some regions, the ionized part of the Orion Bar and NGC 7023 NW, where PAHs and PAHs with less than 50 C atoms are not present, respectively. Hence, to study the effect of PAHs on the derived cosmic-ray ionization rate, we consider four separate cases, without PAHs and with three values of the PAH abundances. We then solve for the cosmic-ray ionization rate and radiation field intensity. The values of ζ for these sightlines differ significantly with and without PAHs.

Our main conclusions from this work are listed below:

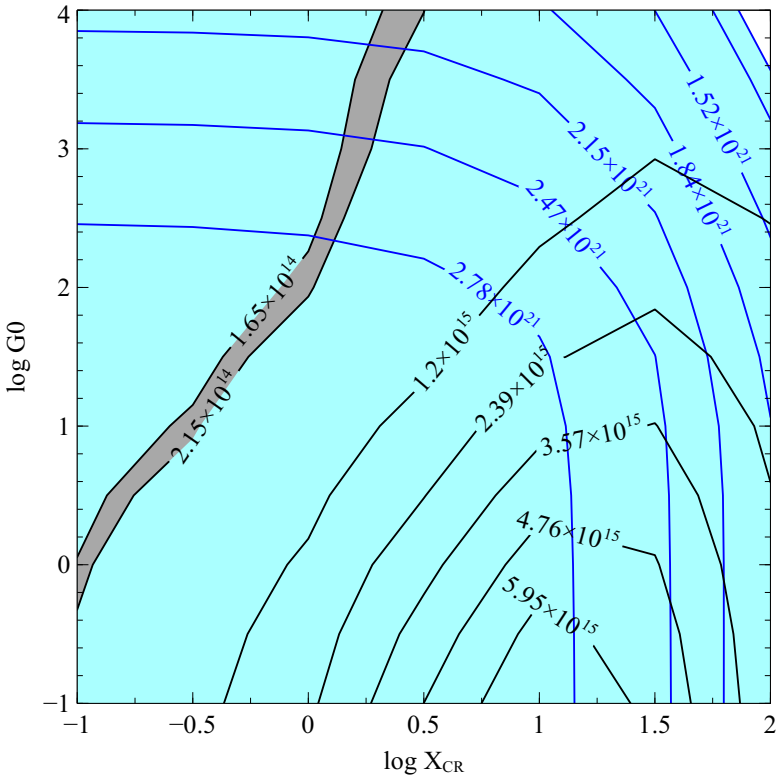

Figure 9. Contour plot of H_3^+ and H_2 as a function of X_{CR} and radiation field (in terms of G0) for HD 204827 with PAH_{avg}. The black and blue solid lines represent contour plots of column densities for H_3^+ and H_2, respectively. The filled areas represent observed column density values $\pm$ 1 σ.

- The common assumption that all carbon is in C^+ in regions where H_3^+ forms is not true in detail. Carbon is mostly C^+ at shallower A_V but becomes neutral or molecules as A_V increases (See Fig.1).

- The common assumption that all electrons are contributed by C^+ where H_3^+ forms is not true in detail. The total electron density is affected by ionization of H^+, S^+, and other metals, and by the effects of PAHs. Hence, e^-/H is not equal to C/H. For instance, we find that, for the Leiden F1 model, $n(e^-)/n(H) > n(C)/n(H)$ (See Fig. 1).

- We show that the electron density depends on the radiation field, the presence of big molecules (PAHs) or very small grains, and ζ. This affects the H_3^+ abundance and derived $\zeta(H_2)$.

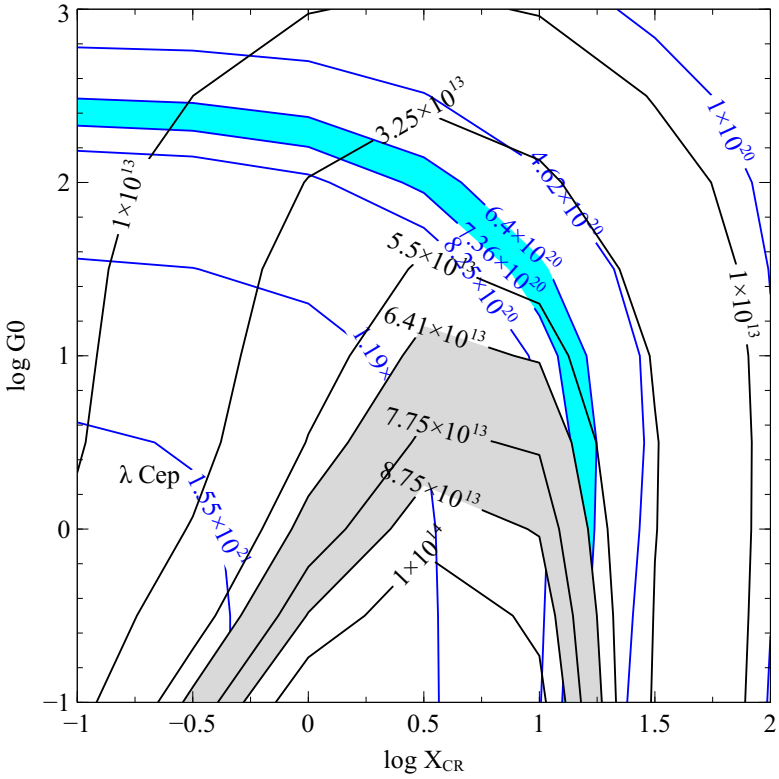

Figure 10. Contour plot of H_3^+ and H_2 as a function of X_{CR} and radiation field (in terms of G0) for λ Cep. The black and blue solid lines represent contour plots of column densities for H_3^+ and H_2, respectively. The filled areas represent observed column density values $\pm$ 1 σ.

- We predict an average cosmic-ray ionization rate $\zeta(H_2)$ equal to $(75.08 \pm 39.90) \times 10^{-16}$ s^{-1}, $(7.88 \pm 2.89) \times 10^{-16}$ s^{-1}, and $(6.50 \pm 3.06) \times 10^{-16}$ s^{-1} for our PAH$_{lo}$, PAH$_{avg}$, and PAH$_{hi}$ cases, respectively, except the two sightlines towards the Cyg OB2 associations.

- We estimate an average value of $\zeta(H_2)$= $(95.69 \pm 46.56) \times 10^{-16}$ s^{-1} for models without PAHs.

- Our derived value of ζ is nearly 1 dex smaller for the sightline towards Cyg OB2 12 than the value predicted by Indriolo & McCall (2012) with PAH$_{avg}$ and PAH$_{hi}$. A much higher rate, approaching the mean of the previous sightlines, is derived when PAHs are not included. This sightline has a highly uncertain H_2 column density. The value of $\zeta(H_2)$ has an uncertainty of more than a dex due to this uncertainty.

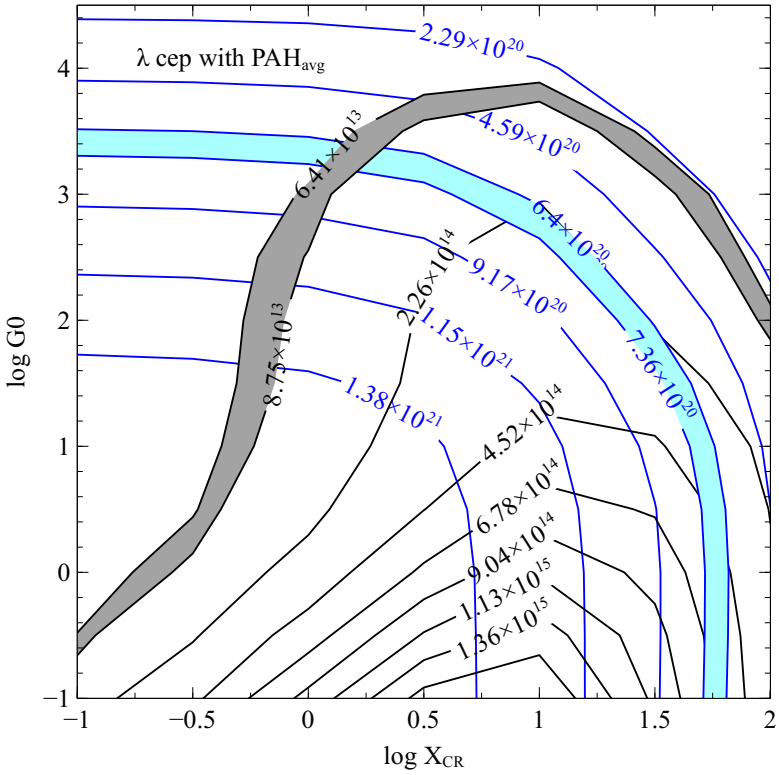

Figure 11. Contour plot of H_3^+ and H_2 as a function of X_{CR} and radiation field (in terms of G0) for λ Cep with PAH_{avg}. The black and blue solid lines represent contour plots of column densities for H_3^+ and H_2, respectively. The filled areas represent observed column density values $\pm$ 1 σ.

ACKNOWLEDGMENTS

GS acknowledges WOS-A grant from Department of Science and Technology (SR/WOS-A/PM-9/2017). GJF acknowledges support by NSF (1816537, 1910687), NASA (ATP 17-ATP17-0141, 19-ATP19-0188), and STScI (HST-AR- 15018). We thank the anonymous referee for his/her thoughtful suggestions.

REFERENCES

Abel, N. P., van Hoof, P. A. M., Shaw, G., Ferland , G. J., & Elwert, T. 2008, ApJ, 686, 1125

Black, J. H. 1987, Heating and Cooling of the Interstellar Gas, ed. D. J. Hollenbach & J. Thronson, Harley A., Vol. 134, 731

Black, J. H., & Dalgarno, A. 1977, ApJS, 34, 405

Carelli, F., Grassi, T., & Gianturco, F. A. 2013, A&A, 549, A103

Cowie, L. L., & Songaila, A. 1986, ARA&A, 24, 499

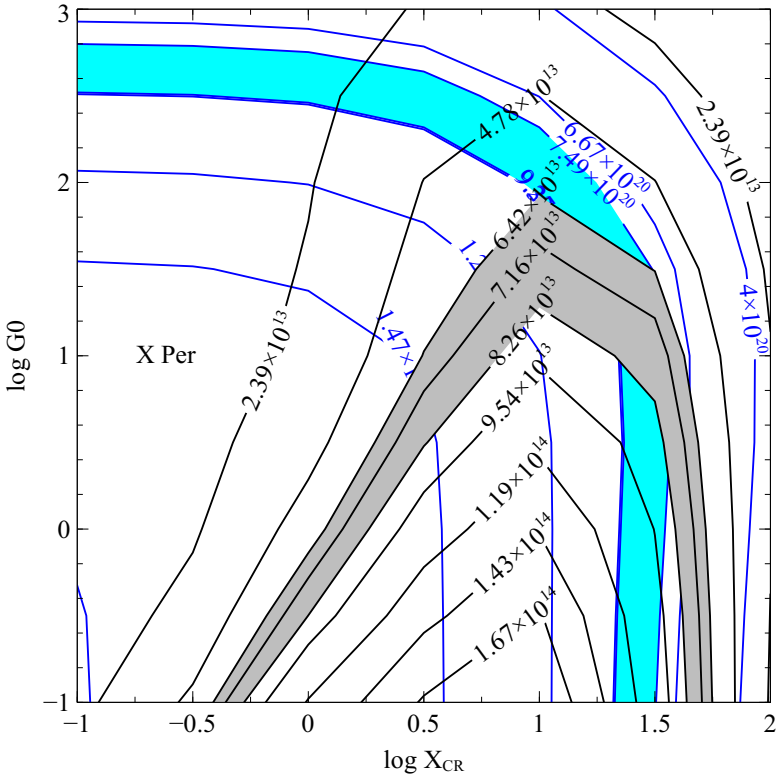

Figure 12. Contour plot of H_3^+ and H_2 as a function of X_{CR} and radiation field (in terms of G0) for X Per. The black and blue solid lines represent contour plots of column densities for H_3^+ and H_2, respectively. The filled areas represent observed column density values $\pm$ 1 σ.

Dalgarno, A. 2006, Proceedings of the National Academy of Science, 103, 12269

Federman, S. R., Weber, J., & Lambert, D. L. 1996, ApJ, 463, 181

Ferland, G. J., Porter, R. L., van Hoof, P. A. M., et al. 2013, RMxAA, 49, 137

Ferland, G. J., Chatzikos, M., Guzmán, F., et al. 2017, RMxAA, 53, 385

Hartquist, T. W., Black, J. H., & Dalgarno, A. 1978, MNRAS, 185, 643

Indriolo, N., Geballe, T. R., Oka, T., & McCall, B. J. 2007, ApJ, 671, 1736

Indriolo, N., & McCall, B. J. 2012, ApJ, 745, 91

Jenkins, E. B. 2009, ApJ, 700, 1299

Klippenstein, S. J., Georgievskii, Y., & McCall, B. J. 2010, Journal of Physical Chemistry A, 114, 278

Le Petit, F., Ruaud, M., Bron, E., et al. 2016, A&A, 585, A105

Li, A., & Draine, B. T. 2001, ApJL, 550, L213

Lykins, M. L., Ferland, G. J., Kisielius, R., et al. 2015, ApJ, 807, 118

Mathis, J. S., Rumpl, W., & Nordsieck, K. H. 1977, ApJ, 217, 425

McCall, B. J., Geballe, T. R., Hinkle, K. H., & Oka, T. 1998, Science, 279, 1910

McCall, B. J., Hinkle, K. H., Geballe, T. R., et al. 2002, ApJ, 567, 391

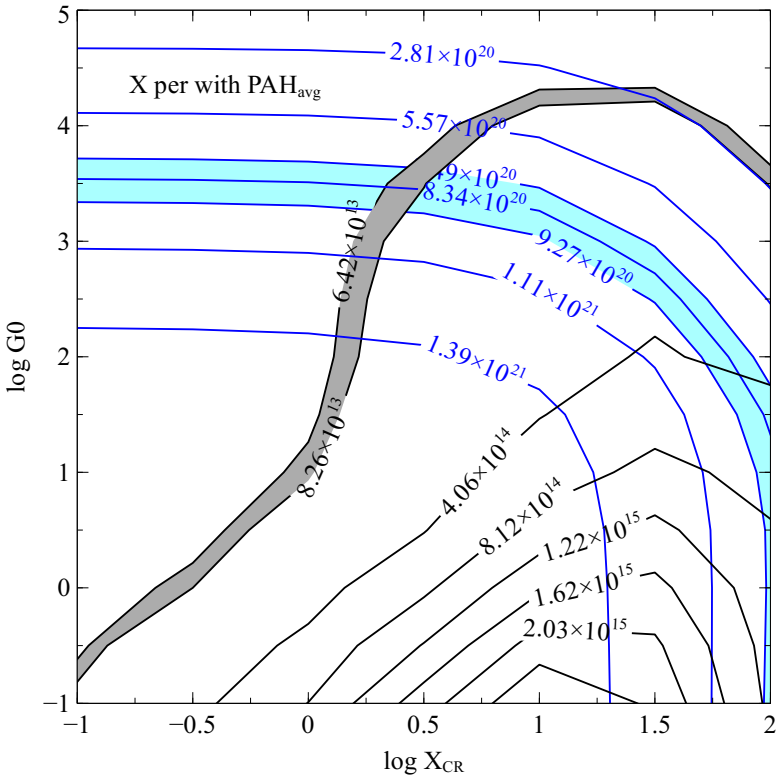

Figure 13. Contour plot of H_3^+ and H_2 as a function of X_{CR} and radiation field (in terms of G0) for X Per with PAH$_{avg}$. The black and blue solid lines represent contour plots of column densities for H_3^+ and H_2, respectively. The filled areas represent observed column density values $\pm$ 1 σ.

McCall, B. J., Huneycutt, A. J., Saykally, R. J., et al. 2003, Nature, 422, 500

—. 2004, PhRvA, 70, 052716

Meyer, D. M., Jura, M., & Cardelli, J. A. 1998, ApJ, 493, 222

Montillaud, J., Joblin, C., & Toublanc, D. 2013, A&A, 552, A15

Neufeld, D. A., & Wolfire, M. G. 2017, ApJ, 845, 163

O'Donnell, E. J., & Watson, W. D. 1974, ApJ, 191, 89

Oka, T., Geballe, T. R., Goto, M., et al. 2019, ApJ, 883, 54

Porter, R. L., Ferland, G. J., Storey, P. J., & Detisch, M. J. 2012, MNRAS, 425, L28

Rachford, B. L., Snow, T. P., Tumlinson, J., et al. 2002, ApJ, 577, 221

Rachford, B. L., Snow, T. P., Destree, J. D., et al. 2009, ApJS, 180, 125

Rakshit, A. B. 1982, International Journal of Mass Spectrometry and Ion Processes, 41, 185

Rawlins, K., Srianand, R., Shaw, G., et al. 2018, MNRAS, 481, 2083

Röllig, M., Abel, N. P., Bell, T., et al. 2007, A&A, 467, 187

Savage, B. D., & Sembach, K. R. 1996, ARA&A, 34, 279

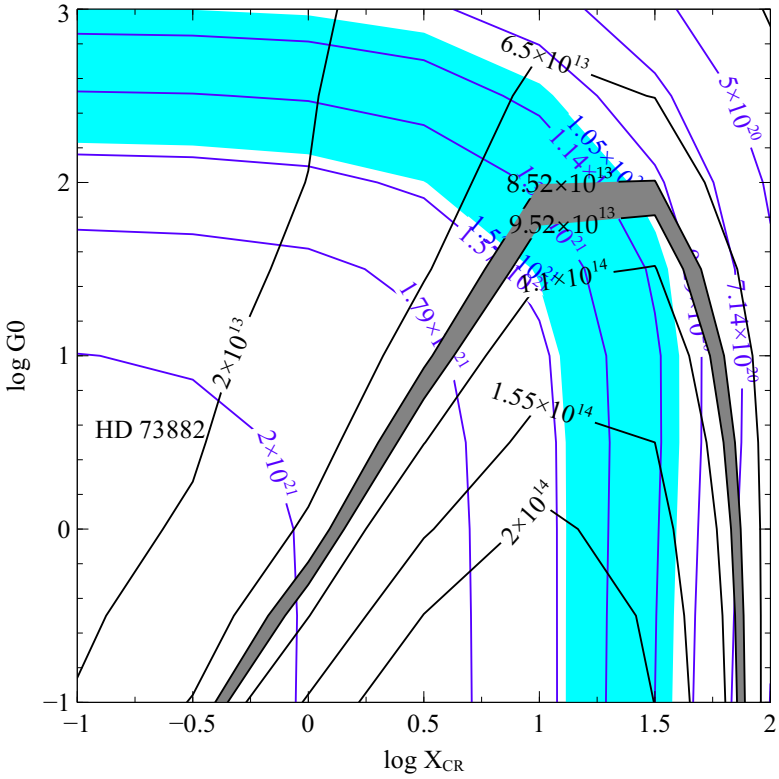

Figure 14. Contour plot of H_3^+ and H_2 as a function of X_{CR} and radiation field (in terms of G0) for HD 73882. The black and blue solid lines represent contour plots of column densities for H_3^+ and H_2, respectively. The filled areas represent observed column density values $\pm$ 1 σ.

Sellgren, K., Tokunaga, A. T., & Nakada, Y. 1990, ApJ, 349, 120

Shaw, G., & Ferland, G. J. 2020, MNRAS, 493, 5153

Shaw, G., Ferland, G. J., Abel, N. P., Stancil, P. C., & van Hoof, P. A. M. 2005, ApJ, 624, 794

Shaw, G., Ferland, G. J., & Ploeckinger, S. 2020, Research Notes of the American Astronomical Society, 4, 78

Shaw, G., Ferland, G. J., Srianand, R., et al. 2008, ApJ, 675, 405

Shaw, G., Rawlins, K., & Srianand, R. 2016, MNRAS, 459, 3234

Snow, T. P., Destree, J. D., & Jensen, A. G. 2007, ApJ, 655, 285

Sonnentrucker, P., Welty, D. E., Thorburn, J. A., & York, D. G. 2007, ApJS, 168, 58

Spitzer, Lyman, J., & Tomasko, M. G. 1968, ApJ, 152, 971

Theard, L. P., & Huntress, W. T. 1974, JChPh, 60, 2840

Thorburn, J. A., Hobbs, L. M., McCall, B. J., et al. 2003, ApJ, 584, 339

Tielens, A. G. G. M. 2008, ARA&A, 46, 289

Tielens, A. G. G. M., & Hollenbach, D. 1985, ApJ, 291, 722

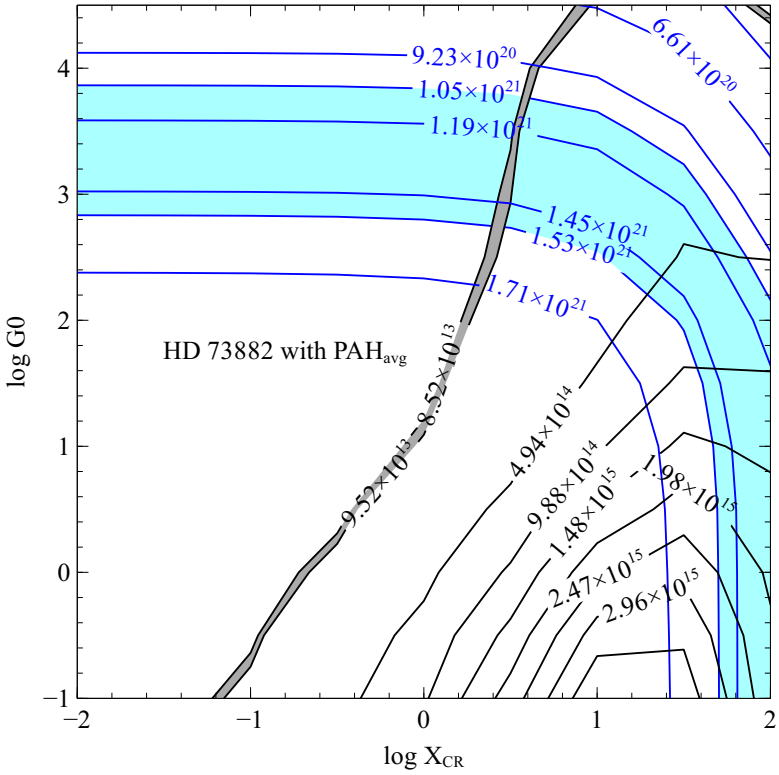

Figure 15. Contour plot of H_3^+ and H_2 as a function of X_{CR} and radiation field (in terms of G0) for HD 73882 with PAH_{avg}. The black and blue solid lines represent contour plots of column densities for H_3^+ and H_2, respectively. The filled areas represent observed column density values $\pm$ 1 σ.

van Dishoeck, E. F., & Black, J. H. 1986, ApJS, 62, 109

Weingartner, J. C., Draine, B. T., & Barr, D. K. 2006, ApJ, 645, 1188

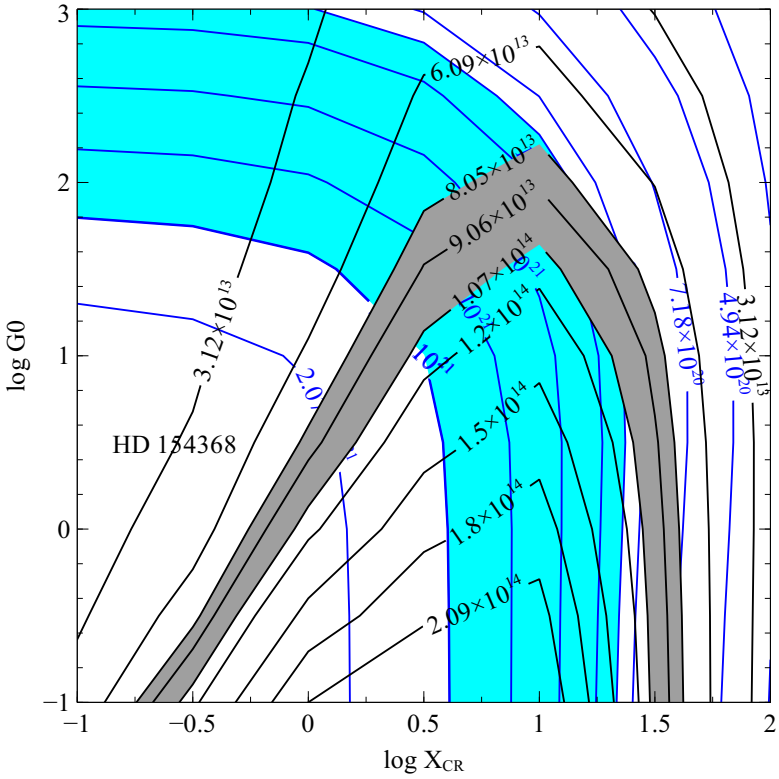

Figure 16. Contour plot of H_3^+ and H_2 as a function of X_{CR} and radiation field (in terms of G0) for HD 154368. The black and blue solid lines represent contour plots of column densities for H_3^+ and H_2, respectively. The filled areas represent observed column density values $\pm$ 1 σ.

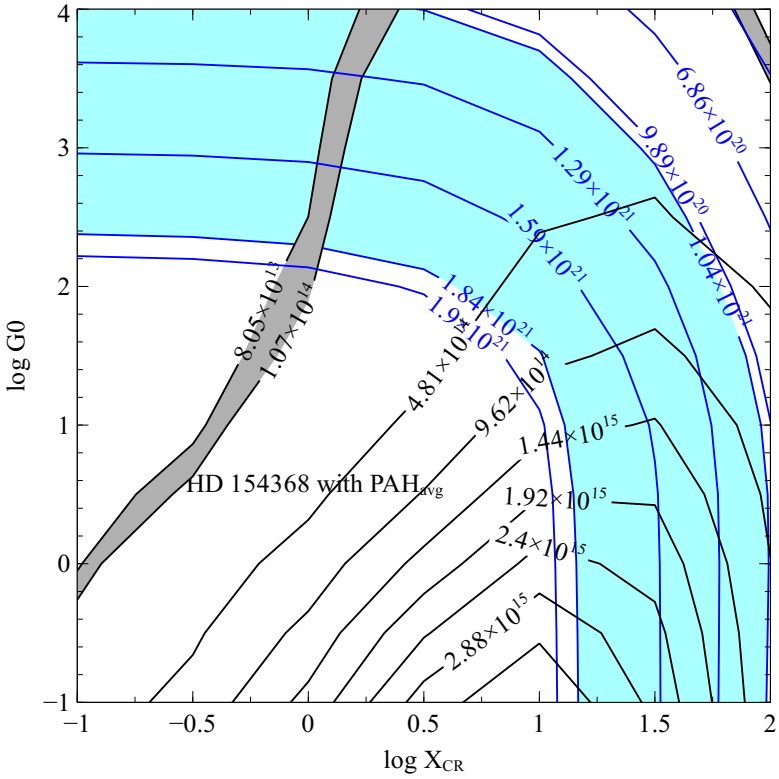

Figure 17. Contour plot of H_3^+ and H_2 as a function of X_{CR} and radiation field (in terms of G0) for HD 154368 with PAH_{avg}. The black and blue solid lines represent contour plots of column densities for H_3^+ and H_2, respectively. The filled areas represent observed column density values $\pm$ 1 σ.

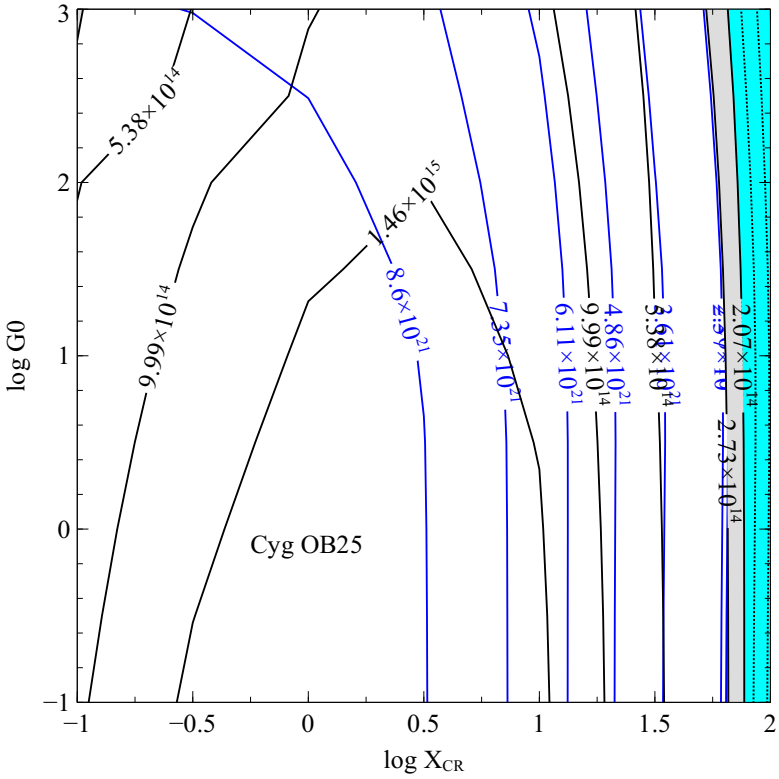

Figure 18. Contour plot of H_3^+ and H_2 as a function of X_{CR} and radiation field (in terms of G0) for Cyg OB2 5. The black and blue solid lines represent contour plots of column densities for H_3^+ and H_2, respectively. The filled areas represent observed column density values $\pm$ 1 σ.

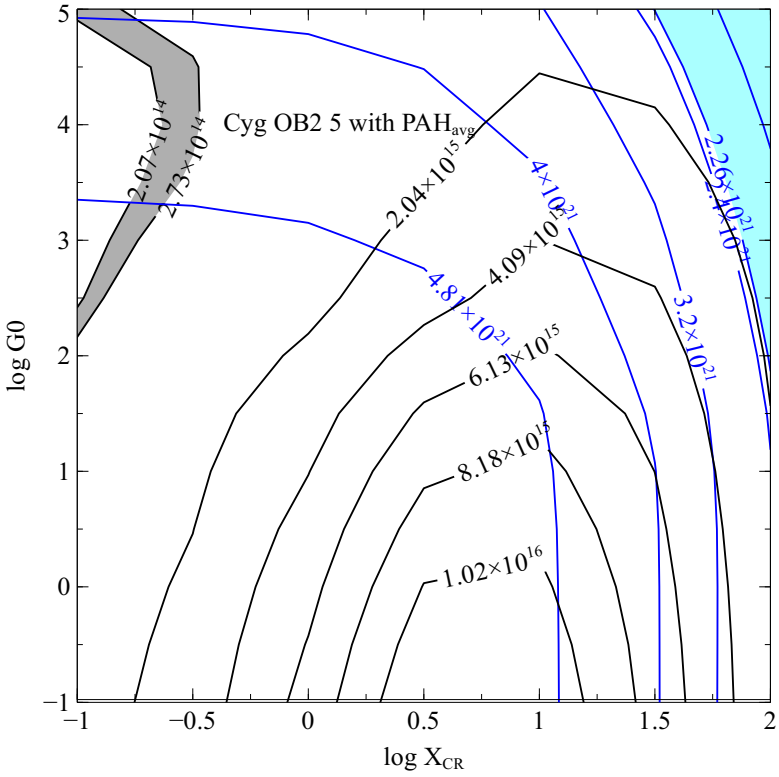

Figure 19. Contour plot of H_3^+ and H_2 as a function of X_{CR} and radiation field (in terms of G0) for Cyg OB2 5 with PAH_{avg}. The black and blue solid lines represent contour plots of column densities for H_3^+ and H_2, respectively. The filled areas represent observed column density values $\pm$ 1 σ. In this case, they do not intersect in the considered parameter space.

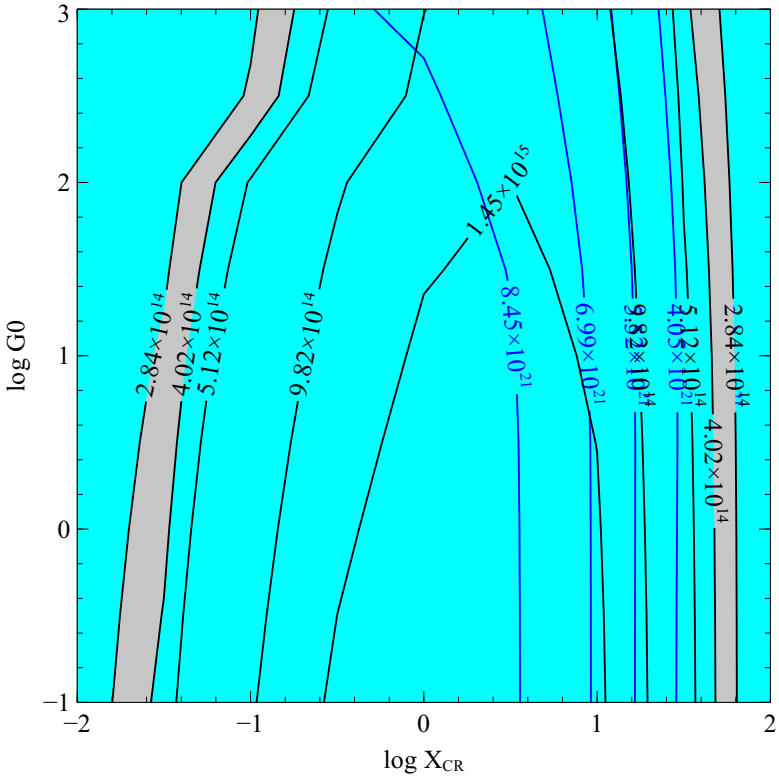

Figure 20. Contour plot of H_3^+ and H_2 as a function of X_{CR} and radiation field (in terms of G0) for Cyg OB2 12. The black and blue solid lines represent contour plots of column densities for H_3^+ and H_2, respectively. The filled areas represent observed column density values $\pm$ 1 σ.

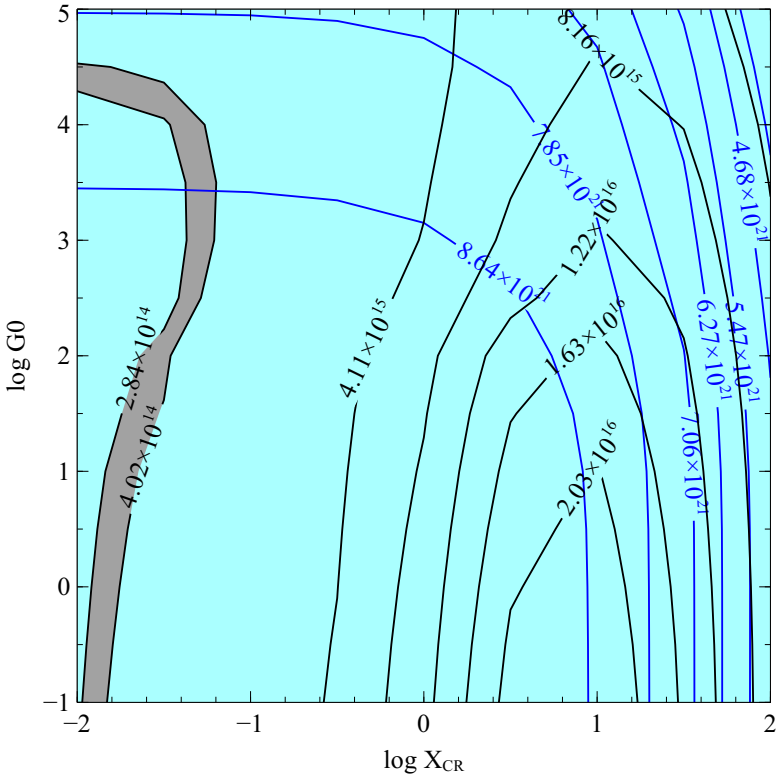

Figure 21. Contour plot of H_3^+ and H_2 as a function of X_{CR} and radiation field (in terms of G0) for Cyg OB2 12 with PAH_{avg}. The black and blue solid lines represent contour plots of column densities for H_3^+ and H_2, respectively. The filled areas represent observed column density values $\pm$ 1 σ.

Table 2. Cosmic ray ionization rate

Objects	$\zeta(H_2)$ this work no PAHs 10^{-16} s^{-1}	$\zeta(H_2)$ this work PAH_{lo} 10^{-16} s^{-1}	$\zeta(H_2)$ this work PAH_{avg} 10^{-16} s^{-1}	$\zeta(H_2)$ this work PAH_{hi} 10^{-16} s^{-1}	$\zeta(H_2) \pm 1\sigma$ Indriolo & McCall (2012) 10^{-16} s^{-1}
HD 169454	2.64 to 5.15	2.41 to 4.47	1.33 to 2.00	0.65 to 0.87	2.45 ± 1.83
HD 110432	≈ 100.48	120.80 to 126.49	7.98 to 11.80	10.04 to 14.86	3.86 ± 2.10
HD 204827	3.73 to 224.93	2.85 to 276.73	0.40 to 12.65	0.15 to 4.92	9.32 ± 6.92
λ Cep	50.35 to 63.40	59.16 to 76.22	4.84 to 8.36	4.81 to 8.55	2.84 ± 1.61
X Per	30.08 to 123.61	29.65 to 152.08	7.57 to 14.86	6.49 to 13.55	5.85 ± 3.54
HD 73882	28.06 to 111.44	24.10 to 89.55	9.59 to 15.92	0.17 to 13.93	9.71 ± 5.57
HD 154368	7.80 to 89.55	6.79 to 79.81	3.41 to 9.59	1.75 to 10.28	4.19 ± 2.62
Cyg OB2 5	219.00 to 303.43	39.08 to 209.92	–	–	8.13 ± 6.03
Cyg OB2 12	0.06 to 258.26	0.04 to 317.73	0.04 to 0.25	0.04 to 0.22	2.93 ± 3.04

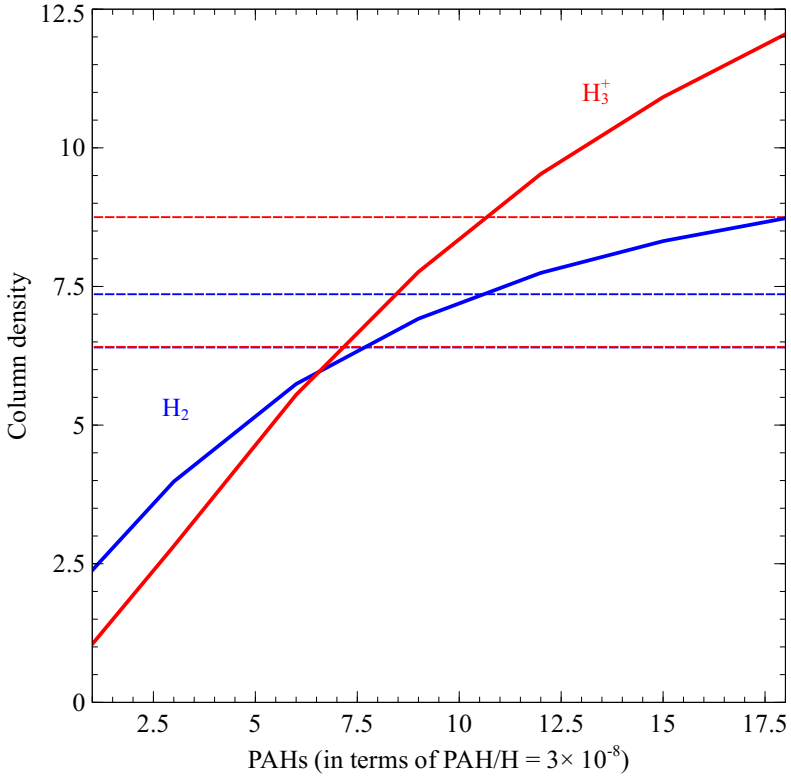

Figure 22. Effect of PAHs on the column densities of H_3^+ and H_2 for the sightline towards λ Cep. The red and blue solid lines represent the predicted column densities for H_3^+ and H_2, respectively. The red and blue dashed-lines represent respective observed column density values $\pm$ 1 σ. Here H_3^+ and H_2 column densities are scaled by 10^{13} and 10^{20}, respectively.